

# Endorepellin remodels the endothelial transcriptome toward a pro-autophagic and pro-mitophagic gene signature

Received for publication, March 14, 2018, and in revised form, May 23, 2018. Published, Papers in Press, June 19, 2018, DOI 10.1074/jbc.RA118.002934

Thomas Neill<sup>‡</sup>, Eva Andreuzzi<sup>§</sup>, Zi-Xuan Wang<sup>‡</sup>, Stephen C. Peiper<sup>‡</sup>,  Maurizio Mongiat<sup>§</sup>, and  Renato V. Iozzo<sup>‡1</sup>

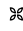
From the <sup>‡</sup>Department of Pathology, Anatomy, and Cell Biology, and the Cancer Cell Biology and Signaling Program, Sidney Kimmel Medical College at Thomas Jefferson University, Philadelphia, Pennsylvania 19107 and the <sup>§</sup>Department of Translational Research, Experimental Oncology Division 2, CRO Aviano-IRCCS, National Cancer Institute, Aviano 33081, Italy

Edited by George N. DeMartino

Regulation of autophagy by proteolytically cleaved fragments of heparan sulfate proteoglycans is a novel and current research focus in tumor biology. Endorepellin is the C-terminal angiostatic fragment of the heparan sulfate proteoglycan perlecan and induces autophagy in endothelial cells. To further investigate this property, we used NanoString, a digital PCR platform for measuring predefined transcripts in biological samples to analyze a custom subset of 95 autophagy-related genes in human umbilical vein endothelial cells treated with ultrapure human recombinant endorepellin. We discovered an endorepellin-evoked pro-autophagic and pro-mitophagic gene expression signatures, which included two coordinately up-regulated mitochondrial-associated genes encoding the E3 ubiquitin protein ligase Parkin and the tumor suppressor mitostatin. Induction of both proteins required the tyrosine kinase activity of vascular endothelial growth factor receptor 2 (VEGFR2). Furthermore, we discovered that endorepellin evoked mitochondrial depolarization in endothelial cells via a specific interaction between its two proximal LG1/2 domains and VEGFR2. We also found that following loss of membrane potential, mitostatin and parkin interact and that mitostatin associates with the established Parkin receptor mitofusin-2. In conclusion, we have identified a critical role for endorepellin in remodeling the autophagic transcriptome and influencing mitochondrial homeostasis.

Autophagic regulation by proteolytically cleaved fragments of heparan sulfate proteoglycans (HSPGs)<sup>2</sup> represent a novel thread of research in tumor biology (1–6) and may represent

This work was supported in part by National Institutes of Health Grants RO1 CA39481 and RO1 CA47282 (to R. V. I.). The authors declare that they have no conflicts of interest with the contents of this article. The content is solely the responsibility of the authors and does not necessarily represent the official views of the National Institutes of Health.

 Author's Choice—Final version open access under the terms of the Creative Commons CC-BY license.

This article contains Figs. S1–S3 and Tables S1 and S2.

<sup>1</sup> To whom correspondence should be addressed: 1020 Locust St., Suite 336, Jefferson Alumni Hall, Thomas Jefferson University, Philadelphia, PA 19107. Tel.: 215-503-2208; Fax: 215-923-7969; E-mail: [renato.iozzo@jefferson.edu](mailto:renato.iozzo@jefferson.edu).

<sup>2</sup> The abbreviations used are: HSPG, heparan sulfate proteoglycan; CCCP, carbonyl cyanide *m*-chlorophenylhydrazine; FCCP, carbonyl cyanide *p*-trifluoromethoxyphenylhydrazine; HAEC, human aortic endothelial cells; HUVEC, human umbilical vein endothelial cells; LC3, microtubule associated light chain 3; LG, laminin G-like domains; PINK1, PTEN-induced putative kinase; p62/SQSTM1, sequestome 1; VEGFR2, vascular endothelial growth factor receptor 2; RTK, receptor tyrosine kinase; GAPDH, glyceraldehyde-3-phosphate dehydrogenase; ANOVA, analysis of variance; EGF, epidermal growth factor.

viable and novel therapeutic opportunities (7) outside conventional roles of the heparan sulfate chains (8–11). Perlecan, which encompass one of the largest multimodular HSPGs found in vascular basement membranes (12–18) and the osteocyte pericellular matrix (19), exhibits angiogenic bivalency by fine-tuning pro- and anti-angiogenic signals (20–22). Endorepellin, the C-terminal domain of perlecan, exhibits potent angiostatic properties (23) and is antithetic in function to the N-terminal HS chains required for growth factor sequestration and co-receptor activity (24, 25). Endorepellin is proteolytically liberated from perlecan *in vivo* (27) by the diverse family of matrix metalloproteinases (28–34). As an example of angiogenic fine tuning, matrix metalloprotease 9 cleaves angiostatic multimerin 2 for vessel sprouting (35).

Structurally, endorepellin is composed of three laminin G-like domains (LG1/3), each separated by twin EGF-like modules (2). Specifically, the modules separating LG2 from LG3 are sensitive to proteolysis and are cleaved by BMP1/Tolloid-like proteases to release the LG3 domain (36). Furthermore, the crystal structure of the C-terminal LG3 domain of endorepellin has been solved (37) and is emerging as an easily accessible biomarker (38) for an ever increasing array of diseases (39–48) including breast cancer (49).

Soluble endorepellin potently “repels” endothelial cell movements, thereby compromising cell migration and capillary morphogenesis (23). At the level of ligand/receptor interactions, endorepellin engages in a “dual receptor antagonism” (50) as a molecular tether, simultaneously ligating VEGFR2 and the  $\alpha 2\beta 1$  integrin (50). The molecular architecture of this heterotrimeric complex has been elucidated (50, 51). The proximal LG1/2 domains interact with the VEGFR2 ectodomain in a region spanning IgG repeats 3–5 (51, 52). In contrast, the terminal LG3 domain interacts with the  $\alpha$ -I domain of the  $\alpha 2$  subunit of the  $\alpha 2\beta 1$  integrin (50), thereby completing the bridge. This complex binding paradigm underscores the exquisite specificity (50) and sensitivity (53) of endorepellin toward endothelial cells. Downstream of dual receptor antagonism, endorepellin attenuates multiple signaling pathways conducive to a pro-angiogenic program via internalization of the receptor complex (4). Concurrent with the inhibition of the phosphatidylinositol 3-kinase/Akt/mammalian target of rapamycin and activation of AMP-activated protein kinase  $\alpha$  (53, 54), we found that endorepellin evokes endothelial cell autophagy downstream of VEGFR2, a process concomitantly

## Endorepellin evokes a pro-autophagic gene signature

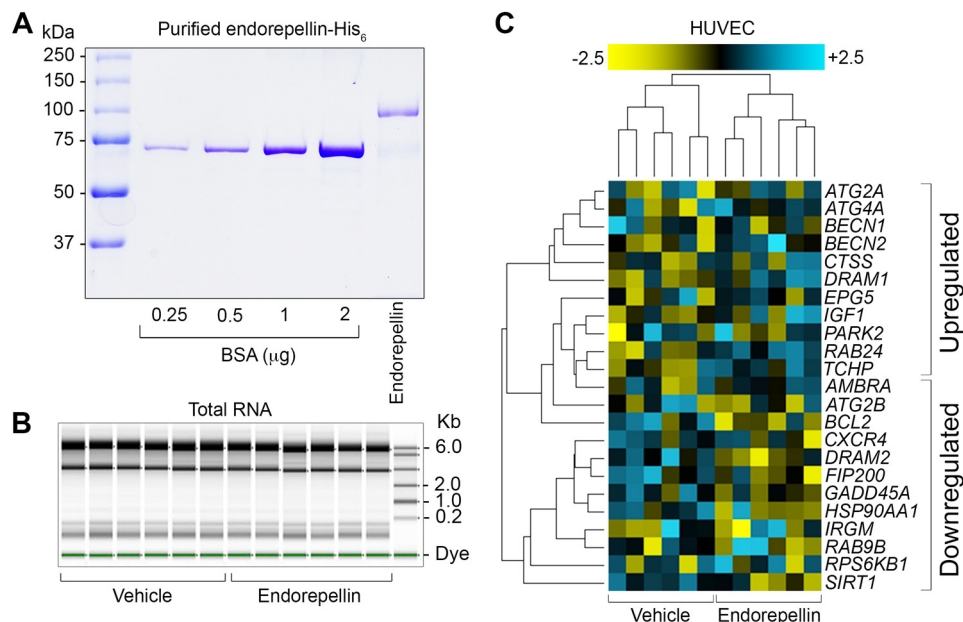


**Figure 1. Endorepellin differentially regulates the autophagic transcriptome.** A, SDS-PAGE demonstrating purity of human recombinant endorepellin. B, Agilent 2200 TapeStation-mediated analysis of RNA integrity and purity via capillary gel electrophoresis. C, hierarchical clustering of the 23 differentially modulated genes that were up-regulated ( $n = 11$ ) or down-regulated ( $n = 12$ ) in HUVEC in vehicle or endorepellin-treated samples. These 23 genes were filtered and selected on two criteria:  $>2$ -fold change (in either directions) and  $p < 0.05$ . Please refer to Tables S1 and S2 for further details. Data in B and C represent 6 independent biological replicates of either vehicle (PBS) or endorepellin (6 h, 200 nM)-treated early-passage (P3) HUVEC.

required for angiostasis (55). During autophagy, endorepellin transcriptionally up-regulates key pro-autophagic genes including *PEG3*, *BECN1*, and *MAP1LC3A* (53). However, a comprehensive understanding of the autophagic transcriptome engaged by endorepellin remains ill-defined.

In this study, we generated a custom NanoString probe-set encompassing 95 autophagy-related genes and probed mRNA of endothelial cells exposed for 6 h to soluble endorepellin. We found a unique endorepellin transcriptomic signature consisting of 23 differentially modulated genes. Of these, two genes, *TCHP* (mitostatin) and *PARK2* (Parkin), were involved in mitochondrial dynamics and mitophagy. We discovered that endorepellin stabilized the PINK1/Parkin quality control system following mitochondrial depolarization downstream of VEGFR2. Moreover, we observed that endorepellin evoked colocalization and binding of mitostatin to Parkin. These findings reveal the depth of endorepellin-evoked endothelial cell autophagy via transcriptome remodeling and open possibilities for extracellular matrix communication to the mitochondria in the regulation of angiostasis.

## Results

### Endorepellin differentially regulates the autophagic transcriptome

Mounting evidence indicates that stable autophagic programs, such as those influenced by endorepellin, require sustained transcriptional responses (56–58). Therefore, we designed a NanoString probe-set to measure the expression of 95 established autophagic genes induced by exposure to nanomolar concentrations of human recombinant endorepellin. NanoString is an innovative, state-of-the-art next generation digital PCR platform that is rapidly gaining attention in many diverse fields. It utilizes unique molecular barcodes to quanti-

tate the number of user-defined transcripts present within each sample (59–63).

Early-passage (P3) human umbilical vein endothelial cells (HUVEC) were treated with highly purified human endorepellin produced in our laboratory (23) expressed in 293-EBNA cells as a C terminus His<sub>6</sub>-tagged protein (Fig. S1A) followed by nickel-nitrilotriacetic acid affinity purification. As determined by SDS-PAGE, our endorepellin preparations were free of any co-purifying contaminants (Fig. 1A). We administered endorepellin in full-serum (nutrient-rich) conditions and extracted total RNA from vehicle (sterile PBS) and endorepellin-treated HUVEC ( $n = 6$ /condition). RNA integrity was analyzed via an Agilent 2200 TapeStation and found to be ultrapure, intact, and suitable for NanoString transcriptomic analyses (Fig. 1B). We identified 23 differentially regulated genes that met our inclusion criteria, 2-fold induction or  $>50\%$  suppression with a concurrent significance of  $p < 0.05$  (Fig. 1C): 11 up-regulated (Table S1) and 12 down-regulated targets (Table S2). The pro-autophagic signature borne out by NanoString provided an unbiased and independent confirmation of endorepellin-evoked *BECN1* transcriptional induction (Fig. 1C) (53) with a simultaneous down-regulation of *BCL2*, a known autophagic inhibitor (Fig. 1C) (64, 65).

We focused on the coordinate up-regulation of *PARK2*, which encodes Parkin, and *TCHP*, which encodes mitostatin. Parkin is widely accepted as an RBR E3-ubiquitin ligase commonly implicated in autosomal-recessive Parkinson's disease (66), and mitostatin is a poorly characterized tumor suppressor gene that we discovered as a decorin-inducible gene in cancer cells (67, 68). Importantly, both Parkin and mitostatin have been implicated in mitochondrial quality control and mitophagy (67, 69–73).

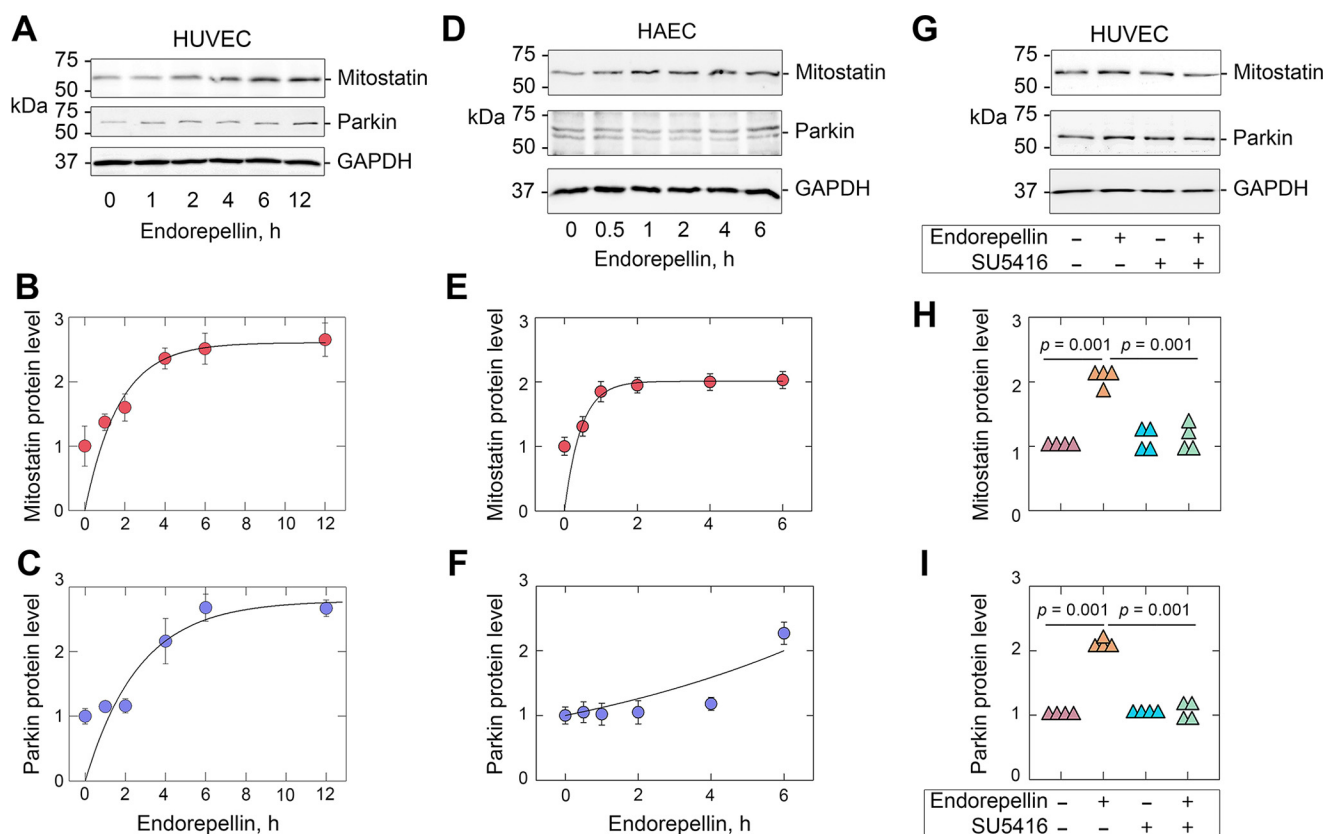


**Figure 2. Endorepellin co-up-regulates mitostatin and Parkin downstream of VEGFR2.** A–C, immunoblot and quantification of mitostatin and Parkin in HUVEC treated with endorepellin over time. D–F, identical experiments as in A–C in HAEC. G–I, immunoblot and quantification of mitostatin and Parkin in HUVEC treated in combination with endorepellin or SU5416 (30  $\mu$ M) for 6 h. GAPDH served as an internal loading control for all immunoblots. Quantifications presented in B, C, E, F, H, and I are representative of at least three to four independent biological replicates in HUVEC or HAEC. Statistical analyses presented in H and I were calculated via one-way ANOVA.

### Endorepellin co-up-regulates mitostatin and Parkin downstream of VEGFR2

We validated the selected NanoString targets by immunoblotting in two different, genetically normal endothelial cell types: HUVEC and Telo-HAEC. The latter are human aortic endothelial cells (HAEC) immortalized by the stable expression of telomerase (hereafter referred to as HAEC). These cell types are comparable in terms of possessing stable genomes, similar exposure to fluid shear stress, and responsiveness to nanomolar concentrations of endorepellin (50, 51, 54, 74).

We found that endorepellin induced mitostatin and Parkin over time (Fig. 2, A–C). In HUVEC, both proteins reached maximal levels at 6 h and remained elevated for up to 12 h. In HAEC, we observed similar kinetics for mitostatin that noticeably increased in as little as 1 h (Fig. 2D) and reached a plateau at ~2 h (Fig. 2, D and E). In contrast, Parkin remained essentially unchanged until the terminal time point (6 h), where the magnitude of Parkin overlapped with that of mitostatin (Fig. 2, D and F).

As endorepellin requires both binding to VEGFR2 as well as its kinase activity to evoke angiostasis and autophagy (4, 21, 75), we next evaluated whether endorepellin would also require VEGFR2 signaling for Parkin and mitostatin up-regulation. We found that blocking the VEGFR2 tyrosine kinase with the selective and reversible ATP-competitive inhibitor, SU5416 (76, 77), significantly abrogated endorepellin-evoked Parkin and mito-

statin induction (Fig. 2, G–I). Taken together, these results indicate a time-dependent increase in endorepellin-evoked Parkin and mitostatin, with differing kinetics, in HUVEC and HAEC downstream of VEGFR2.

### Endorepellin evokes mitochondrial depolarization via LG1/2

It is well established that Parkin is recruited to depolarized and/or damaged mitochondria (66, 79, 80). Thus, we hypothesized that endorepellin could compromise mitochondrial membrane potential integrity via Parkin modulation. We assessed the effects of endorepellin on mitochondrial membrane potential ( $\Delta\Psi_m$ ) using JC-1, a lipophilic cationic dye that is sensitive to voltage fluctuations. JC-1 accumulates within the inner mitochondrial membrane in response to the  $\Delta\Psi_m$ . At a low  $\Delta\Psi_m$  (e.g. loss of membrane potential), JC-1 is monomeric and exhibits green fluorescence. However, high levels of JC-1 accumulate (proportional to a high  $\Delta\Psi_m$ ) and lead to the formation of JC-1 aggregates that shifts the JC-1 emission spectrum toward red fluorescence (81). To this end, we treated HUVEC with endorepellin in parallel with carbonyl cyanide *m*-chlorophenylhydrazine (CCCP) or carbonyl cyanide *p*-trifluoromethoxyphenylhydrazone (FCCP), both known ionophores that uncouple ATP synthesis by transporting hydrogen ions across the mitochondrial membranes and dissipating the proton motive force.



## Endorepellin evokes a pro-autophagic gene signature

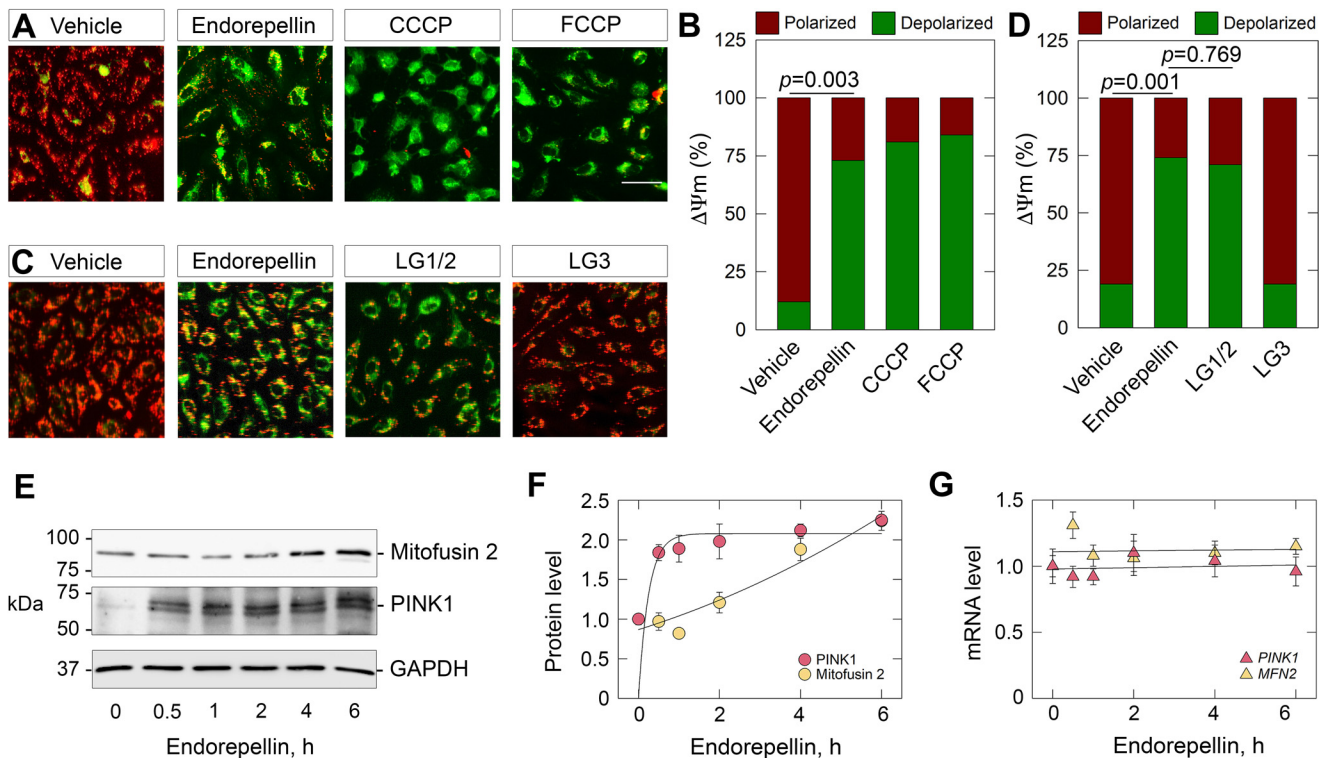


**Figure 3. LG1/2 domain of endorepellin is sufficient for mitochondrial depolarization.** A and B, representative fluorescence micrographs depicting live cell imaging of HUVEC after incubation with endorepellin (6 h), CCCP (1 h, 30  $\mu$ M), or FCCCP (10 min, 500 nM) in A, or endorepellin (6 h), LG1/2 (6 h, 150 nM), or LG3 (6 h, 150 nM) in B. HUVEC were cultured in nutrient-rich media and incubated with JC-1 (20 min, 7.5  $\mu$ M) to assess mitochondrial membrane potential. Scale bar  $\sim$ 80  $\mu$ m. C and D, quantification of polarized (green) compared with depolarized (red) mitochondria as shown in A or B, respectively. E and F, immunoblot and quantification of mitofusin 2 and PINK1 in HUVEC treated with endorepellin over time. G, analyses of PINK1 or MFN2 in HUVEC treated with endorepellin over time. For live cell imaging in A and B, at least 10 fields per condition were acquired for each of three to four biological replicates in HUVEC. Quantifications in C and D are representative of three to four independent biological replicates. GAPDH served as an internal loading control for immunoblots in E and are representative of four independent biological replicates. Immunoblot quantifications in F are representative of four independent biological replicates. Gene expression analyses presented in G have been normalized to ACTB and represent four independent biological replicates. Statistical analyses presented in C and D were calculated via one-way ANOVA.

We found a profound loss of  $\Delta\Psi_m$  as determined by JC-1 staining (Fig. 3A) and further quantification of the green (depolarized, JC-1 monomers) and red (polarized, JC-1 aggregates) fluorescence (Fig. 3B). The magnitude of depolarization was not significantly different between endorepellin and CCCP ( $p = 0.652$ ) or endorepellin and FCCCP ( $p = 0.443$ ), indicating comparable  $\Delta\Psi_m$  efficiency and a potential common pathway.

In an effort to identify the domains required for endorepellin binding to VEGFR2 (51), we generated two endorepellin fragments containing LG1/2 (composed of LG1, LG2, and both sets of the twin EGF-like modules) (Fig. S1A) or simply LG3 alone (Fig. S1A). We have previously shown that LG1/2 binds the IgG<sub>3-5</sub> repeats of the VEGFR2 ectodomain, whereas LG3 binds the  $\alpha\beta1$  integrin (4, 52, 75, 82). Thus, we employed these fragments to dissect which bioactive modules of endorepellin are responsible for transducing  $\Delta\Psi_m$  pertinent information. Notably, LG1/2 resulted in a robust  $\Delta\Psi_m$  akin to endorepellin (Fig. 3C). In contrast, LG3 was unable to evoke such a response (Fig. 3C). Quantifying the fluorescence intensity for both channels, we found a significant depolarization upon LG1/2 treatment (Fig. 3D) that was not statistically significantly different from endorepellin ( $p = 0.769$ ), whereas LG3 was unchanged relative to control levels ( $p = 0.905$ ). As  $\Delta\Psi_m$  was unchanged by LG3, we surmised blocking the  $\alpha\beta1$  integrin with a specific mAb, mAb1998Z (53, 83), should have no apparent effect on

endorepellin-evoked mitochondrial depolarization. Intriguingly, we found that endorepellin in the presence of mAb1998Z prevented  $\Delta\Psi_m$  when compared with endorepellin alone (Fig. S2, A and D). We validated endorepellin and mAb199Z with phalloidin staining to visualize the actin cytoskeleton. Endorepellin evokes actin dissolution via the  $\alpha\beta1$  integrin (83), specifically LG3 (51, 82). Indeed, abrogating binding of endorepellin to the  $\alpha\beta1$  integrin inhibited actin dissolution (Fig. S2B), thereby functionally validating mAb1998Z. Next, we combined LG1/2 with mAb1998Z and found loss of membrane potential independent of the  $\alpha\beta1$  integrin blocking activities of the antibody (Fig. S2, C and E). Collectively, these data reinforce the concept that VEGFR2 is the primary receptor for endothelial cell  $\Delta\Psi_m$ , irrespective of the  $\alpha\beta1$  integrin. These data indicate that LG1/2 is sufficient for mitochondrial depolarization and is most likely transduced by VEGFR2.

### Endorepellin-evoked modulation of PINK1 and mitofusin 2

Having established that endorepellin compromises  $\Delta\Psi_m$ , we next examined whether endorepellin would also affect PINK1, an effector kinase stabilized in response to mitochondrial depolarization (84), which works in synergy with Parkin (66). Among the targets of PINK1 is mitofusin 2 that acts as a receptor for recruited Parkin to cull damaged mitochondria (85). We found a rapid and sustained accumulation of PINK1 (within 30 min) following

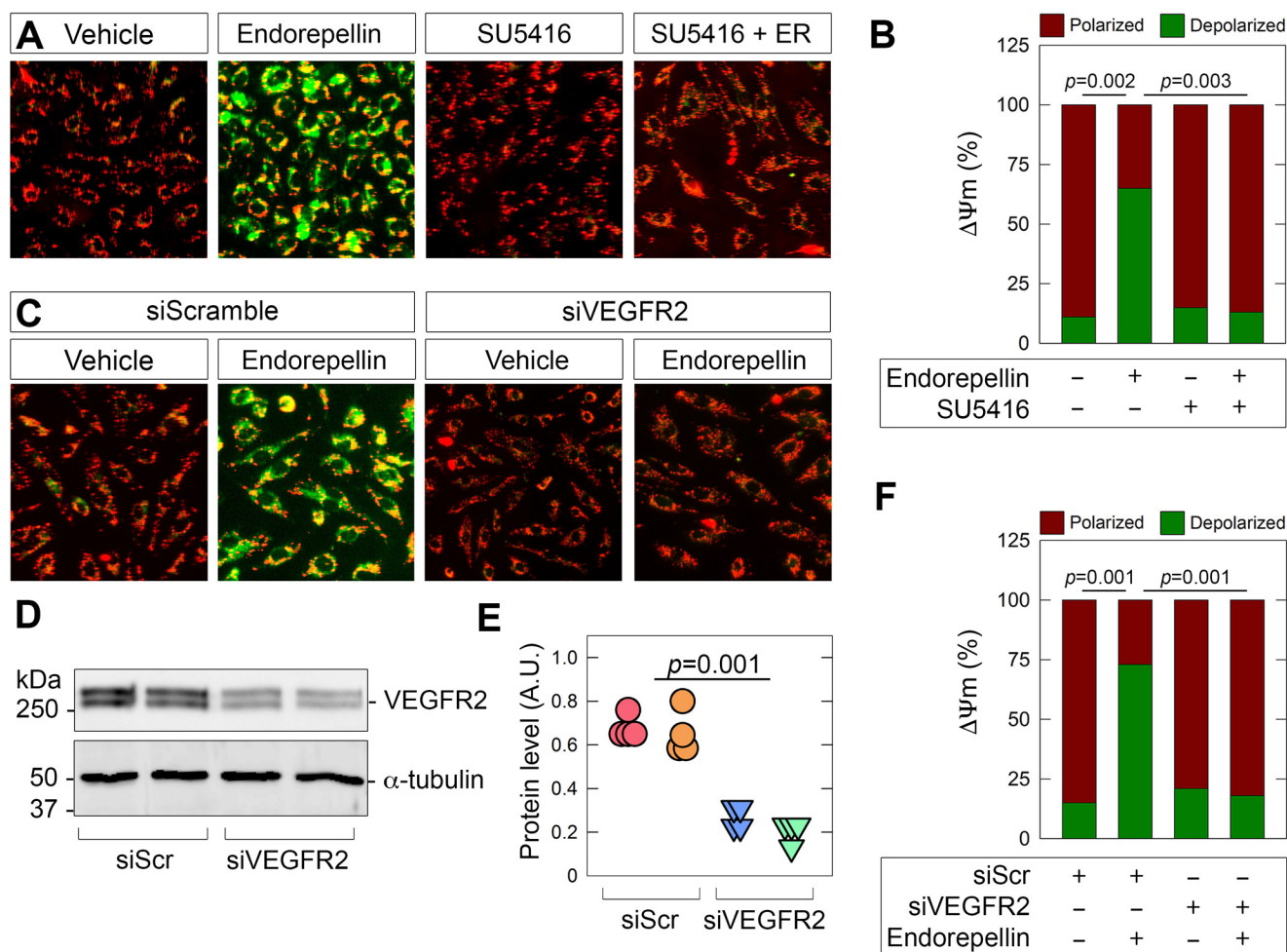


**Figure 4. VEGFR2 is required for endorepellin-evoked mitochondrial depolarization.** *A*, representative fluorescence micrographs depicting live cell imaging of HUVEC after incubation with endorepellin in combination with SU5416 after staining with JC-1. HUVEC were cultured in nutrient-rich media. *B*, quantification of polarized (green) compared with depolarized (red) mitochondria as shown in *A*. *C*, representative fluorescence micrographs depicting live cell imaging of HUVEC after transient transfection of scramble siRNA (siScramble) or siVEGFR2 followed by endorepellin (6 h). *D* and *E*, immunoblot and quantification of VEGFR2 silencing in HUVEC. *F*, quantification of polarized (green) compared with depolarized (red) mitochondria as shown in *C*. Scale bar in *A* and *C*, ~80  $\mu$ m. For live cell imaging in *A* and *C*, at least 10 fields per condition were acquired for each of four biological replicates in HUVEC. Quantifications in *B* and *F* are representative of four independent biological replicates. GAPDH served as an internal loading control for immunoblots in *D* and are representative of four independent biological replicates. Immunoblot quantifications in *E* are representative of four independent biological replicates. Statistical analyses presented in *B* and *F* were calculated via one-way ANOVA.

endorepellin treatments (Fig. 3, *E* and *F*). This was followed, at later time points, by a concomitant accumulation of mitofusin 2 protein (Fig. 3, *E* and *F*). We complemented these results in HUVEC with CCCP and FCCP and found comparable increases in both PINK1 over time with CCCP (Fig. S1*B*) and PINK1 transiently with FCCP (Fig. S1*C*) in HUVEC. Notably, these increases in PINK1 and mitofusin 2 occurred independently of transcription, as no modulation in the mRNA profiles of either *PINK1* or *MFN2* was found (Fig. 3*G*). Thus, we have identified a novel downstream signaling pathway for endorepellin that triggers mitochondrial depolarization via the LG1/2 domain with a consequent increase in PINK1 and mitofusin 2, independent of transcription.

#### VEGFR2 is required for endorepellin-evoked mitochondrial depolarization

Having ascertained that LG1/2 is sufficient for mitochondrial depolarization, we evaluated whether the tyrosine kinase of VEGFR2 is required. Using JC-1 to assess the effects of endorepellin on  $\Delta\Psi_m$ , we found that blocking VEGFR2 kinase

with SU5416 significantly blocked endorepellin-evoked  $\Delta\Psi_m$  (Fig. 4, *A* and *B*). Furthermore, treatment with SU5416 alone had no effect, suggesting an active process mediated exclusively upon endorepellin-binding VEGFR2 (Fig. 4, *A* and *B*). Next, we utilized siRNA to transiently deplete VEGFR2. Transient transfection of a scramble siRNA sequence complexed with a lipid-based carrier did not cause significant damage or undue stress (compare Fig. 4, *A* with *C*). After validating VEGFR2 depletion with a pool of 3–5 targeting siRNA oligonucleotides (Fig. 4*D*) with a resulting knockdown of ~65% (Fig. 4*E*), we found that loss of the receptor recapitulated the effect of pharmacological inhibition with SU5416 (Fig. 4*C*) and significantly attenuated  $\Delta\Psi_m$  (Fig. 4*F*). Thus, we have identified a functional and mechanistic role for VEGFR2 in transducing information from endorepellin for mitochondrial depolarization in endothelial cells.

#### Parkin and mitostatin colocalize in a VEGFR2-dependent manner

Next, we utilized confocal laser microscopy to determine whether there is any co-localization of Parkin, and mitostatin,



## Endorepellin evokes a pro-autophagic gene signature

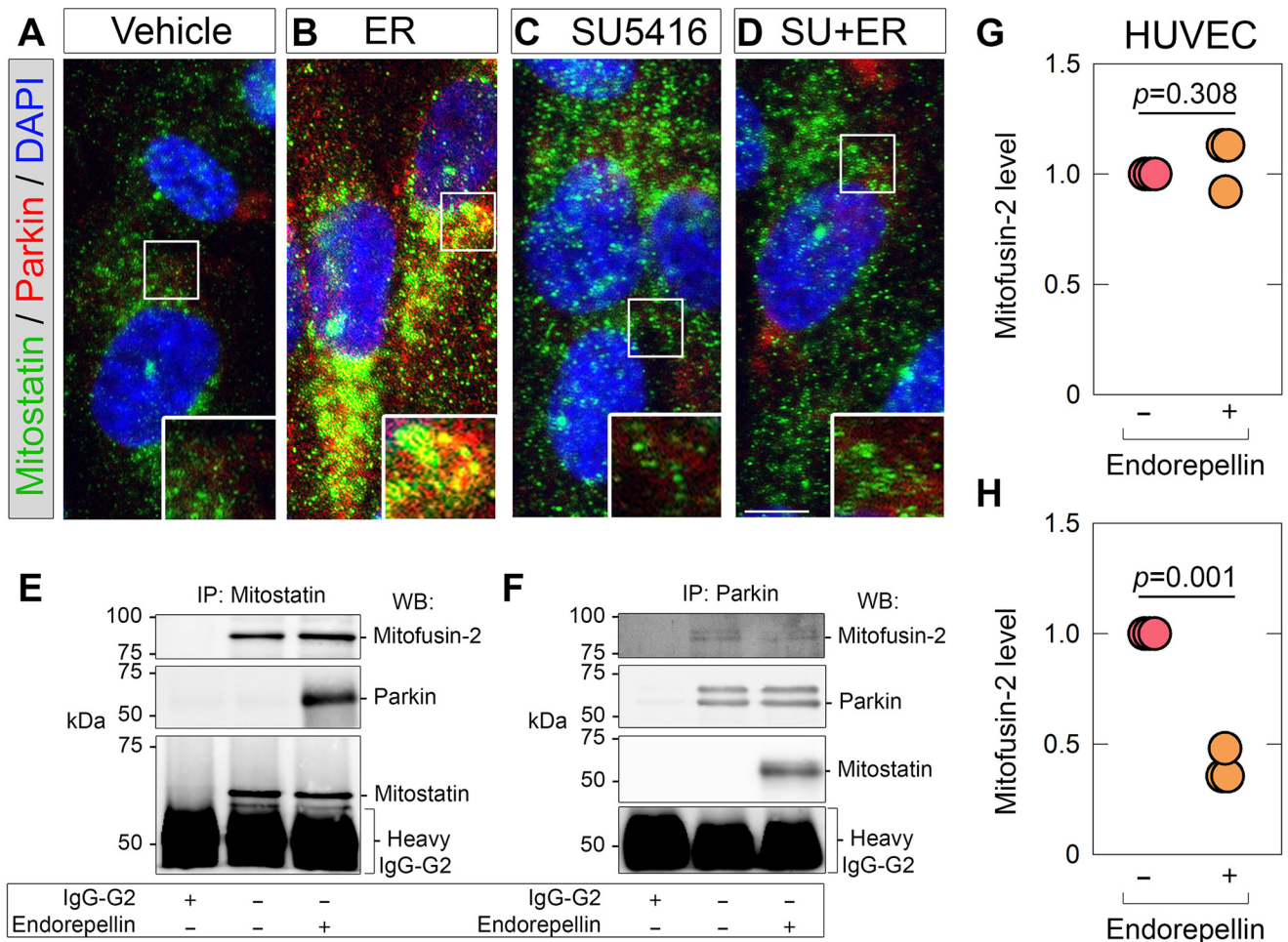


**Figure 5. Parkin and mitostatin co-localize in a VEGFR2-dependent manner.** A–D, confocal laser microscopy depicting mitostatin (green) and Parkin (red) following endorepellin (6 h) alone or in combination with SU5416 in HUVEC. Nuclei (blue) were visualized with 4',6-diamidino-2-phenylindole (DAPI). Scale bar ~10 mm. Insets denote 3 times digitally magnified images from the area demarcated by the solid white box. E and F, representative images of co-immunoprecipitations of HUVEC treated with endorepellin and immunoprecipitated for mitostatin (E) or Parkin (F) and immunoblotted for mitofusin 2, Parkin, or mitostatin. G and H, quantification of mitofusin-2 following mitostatin immunoprecipitation (as in E) or Parkin immunoprecipitation (as in F). For confocal microscopy in A–D, at least five fields/condition were obtained for at least two independent biological replicates in HUVEC. Immunoblots in E and F are representative of three independent biological replicates in HUVEC. Mitofusin-2 quantifications in G and H are representative of three independent biological replicates in HUVEC. Statistical analyses provided by two-tailed Student's *t* test.

and whether mitostatin and Parkin interact in solution. Moreover, mitostatin binds mitofusin 2 at specialized regions known as mitochondrial associated membranes juxtapositions between the mitochondria and endoplasmic reticulum (86).

Under basal conditions, we detected very little Parkin staining (Fig. 5A) in agreement with the biochemical data showing low levels detected by immunoblot (cf. Fig. 2A). Mitostatin immunoreactivity was considerably more robust with a profuse staining pattern throughout the cell and nuclear compartments (Fig. 5A). We found no co-localization of mitostatin and Parkin under resting conditions. Exogenous endorepellin caused a marked increase in Parkin throughout the cytosol and a striking co-localization of mitostatin and Parkin (Fig. 5B) in clearly delineated punctate structures (Fig. 5B, inset). As seen above with the  $\Delta\Psi_m$  assays, SU5416 alone had no effect on the distribution of mitostatin and Parkin (Fig. 5C). However, SU5416 completely blocked the effect of endorepellin on mitostatin and Parkin co-localization (Fig. 5D). These data suggest that VEGFR2 controls the association of mitostatin and Parkin in response to endorepellin.

Next, we corroborated our imaging study with immunoprecipitation data. Using the anti-mitostatin antibody, we successfully immunoprecipitated mitostatin. Lysates exposed to a control rabbit IgG-G2 displayed no such immunoprecipitates (Fig. 5E), validating the specificity of our antibody. Importantly, we found an exclusive interaction of mitostatin with Parkin following endorepellin treatment (Fig. 5E), thereby confirming our confocal microscopy results. We also confirmed the previously reported (86) basal association of mitostatin with mitofusin 2 (Fig. 5E) but found no altered interactions upon endorepellin treatment (Fig. 5E).

Next, we performed reciprocal co-immunoprecipitations of Parkin (Fig. 5F). Using a control mouse IgG-G2, we found no immunoprecipitating bands, substantiating the specificity of our antibody. In agreement with the immunofluorescence data, we found an exclusive association of Parkin with mitostatin following endorepellin treatment (Fig. 5F). However, immunoblotting for mitofusin 2 revealed a modest decrease in the association of Parkin and mitofusin 2 not seen when mitostatin was immunoprecipitated (Fig. 5F). These data suggest a differential

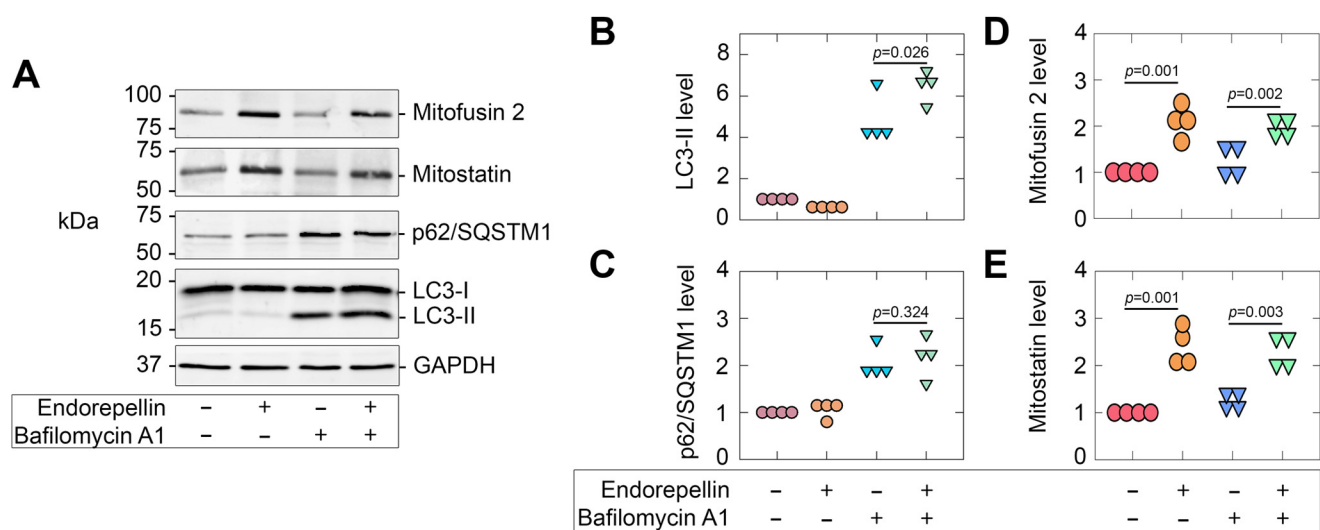


**Figure 6. Endorepellin evokes autophagic flux, but not of mitofusin 2 or mitostatin.** A, representative immunoblots of mitofusin 2, mitostatin, p62/SQSTM1, LC3-I/-II, and GAPDH following endorepellin (6 h) alone or in combination with bafilomycin A1 (100 nM). B–E, quantification of targets as shown in A. GAPDH served as an internal loading control for immunoblots in A and are representative of four independent biological replicates. Immunoblot quantifications in B–E are representative of four independent biological replicates. Statistical analyses presented in B and C were calculated via one-way ANOVA.

binding of mitostatin and mitofusin 2 over Parkin in endothelial cells. Quantification of mitofusin-2 following immunoprecipitation of mitostatin (Fig. 5G) or Parkin (Fig. 5H) further confirmed these results.

Collectively, our results identify an exclusive association between mitostatin and Parkin after exposure to endorepellin. Furthermore, the formation of the mitostatin-Parkin complexes require the physical presence of VEGFR2 and the activity of its kinase.

#### Endorepellin evokes autophagic flux, but not of mitofusin 2 or mitostatin

We have determined that endorepellin is capable of increasing the rate of endothelial cell autophagy (55) by examining autophagic flux of established markers (such as LC3-II) (87) in the presence of chloroquine. Here, we evaluated the effects of bafilomycin A1, a V-type ATPase inhibitor that prevents fusion between the autophagosome and lysosome, in conjunction with endorepellin thereby permitting analyses of the rates of accumulated autophagic markers. Treatment with bafilomycin A1 (100 nM) alone resulted in a marked accumulation of LC3-II (Fig. 6, A and B) and p62/SQSTM1 (Fig. 6, A and C). Intriguingly, under basal conditions at two different concentrations, bafilomycin A1 had no discernible effects on mitofusin 2 (Fig. 6, A and D) or mitostatin (Fig. 6, A and E).

In congruence with our previous study (55), endorepellin, in combination with bafilomycin A1, significantly enhanced autophagic flux as per LC3-II analysis (Fig. 6, A and B). However, under the same conditions, we found no significant increase (or change) in the levels of p62/SQSTM1 (Fig. 6, A and C). Likewise, as per the aforementioned data (cf. Figs. 2 and 3E), endorepellin evoked mitofusin 2 (Fig. 6, A and D) and mitostatin (Fig. 6, A and E). Intriguingly, a combination treatment of endorepellin and bafilomycin A1 increased neither mitofusin 2 (Fig. 6, A and D) nor mitostatin (Fig. 6, A and E) above that of simply endorepellin alone. Parkin responded in a similar manner (data not shown).

In summary, we recapitulated endorepellin-enhanced autophagic flux in endothelial cells. However, the newly identified targets were not sensitive to basal autophagic flux nor augmented flux as stimulated by endorepellin.

#### Discussion

We discovered a unique endorepellin-evoked autophagic signature following digital PCR profiling of a specific subset of the endothelial cell transcriptome. Querying our custom probe-set, we found 23 differentially regulated genes. Among the targets, several genes including the distinct regulation of *BECN1* and the autophagic inhibitor *BCL2* (53, 64, 65, 88, 89) independently confirmed the robustness of our dataset and signals a shift to a pro-autophagic program. Beclin-1 is phosphorylated by Akt leading to autophagic inhibition (90). We discovered that endorepellin inactivates the phosphatidylinositol 3-kinase/Akt pathway (54) as a potential mechanism of Beclin 1 derepression and resultant autophagic initiation. Beclin 1 appears to be governed by RTKs (91), designating a convergence on RTKs by soluble matrix components in evoking autophagy (92). The Beclin-1 homologue *BECN2*, also implicated in autophagy and metabolism (93), was further identified as an endorepellin-inducible gene.

Moving forward, endorepellin co-up-regulates the mRNA and protein of *PARK2* and *TCHP* (encoding Parkin and mitostatin, respectively), effectors implicated in mitochondrial homeostasis and mitophagy (66, 73). Induction of Parkin and mitostatin depended on the VEGFR2 tyrosine kinase, indicating partial agonism, thereby allowing us to refine the model as a “dual receptor partial agonism” rather than strict dual receptor antagonism.

Given that Parkin is recruited to depolarized and/or damaged mitochondria for Parkin-mediated mitophagy (94), we discovered that endorepellin-evoked mitochondrial depolarization. Intriguingly, depolarization occurred with the same magnitude as CCCP and FCCP, known electron transport chain uncouplers. Functionally, and mechanistically, the mod-

## Endorepellin evokes a pro-autophagic gene signature

ular architecture of endorepellin permitted us to identify the LG1/2/VEGFR2 interaction, but not the LG3/ $\alpha$ 2 $\beta$ 1 interaction, as sufficient for the loss of mitochondrial membrane potential. Intriguingly, a combination of mAb1998Z with endorepellin significantly blocked  $\Delta\Psi_m$ . This might be due to a positioning role of the  $\alpha$ 2 $\beta$ 1 integrin for full-length endorepellin to interact with VEGFR2. This is reinforced by LG1/2 in conjunction with mAb1998Z efficiently depolarizing the mitochondria and lack of response of LG3 alone. Alternately, endorepellin may have been blocked due to steric hindrance from the antibody binding to the  $\alpha$ 1-domain of the  $\alpha$ 2 subunit and unabridged endorepellin.

Whether mitochondrial depolarization occurs downstream of VEGFR2 in response to intracellular calcium mobilization (95, 96) remains unknown. However, based on our previous work (54) this mode of action seems unlikely. Endorepellin prevents phosphorylation of VEGFR2 at Tyr<sup>1175</sup>, a key phosphosite for phospholipase C- $\gamma$  recruitment; thereby, precluding the formation of diacylglycerol and inositol 1,4,5-triphosphate. The latter being critical for calcium flux downstream of RTK signaling. Concurrent with mitochondrial depolarization was a rapid stabilization of PINK1 (94) and temporal accumulation of mitofusin 2, a mitostatin binding partner and Parkin receptor (85, 86, 97). Increased amounts of mitofusin 2 act to juxtapose Parkin near PINK1 for subsequent activation (97) and clearance of the damaged organelle.

The co-localized mitostatin/Parkin positive puncta formed in response to endorepellin, downstream of VEGFR2 signaling, was decidedly more discreet in morphology than autophagosomes evoked by endorepellin (53, 55). This interaction appeared to form only after stimulation, as no co-localization or binding was found under basal conditions. Using the previously published interaction between mitostatin and mitofusin 2 (86) as a positive control for our immunoprecipitation, we found an increased association between mitostatin and mitofusin 2 post-endorepellin treatment. Resolving the precise interactions and deciphering the biological consequence of the mitostatin/Parkin interaction and increased binding of mitostatin to mitofusin 2 will require future studies as it pertains to mitochondrial homeostasis.

The observation that Parkin, mitostatin, and mitofusin 2 are not substrates of basal autophagic flux or endorepellin-evoked flux in endothelial cells implies their function in an alternate pathway. Indeed, mitofusin 2, despite being involved in mitophagy, is sent to the 26S proteasome for degradation by Parkin (70). Emerging evidence posits a cooperation between the autophagic machinery and the ubiquitin-proteasome system for competent mitochondrial clearance via mitophagy (98). Considering that mitostatin-Parkin and mitostatin-mitofusin 2 are complexed, these protein complexes may thereby bypass the autophagosomal system and are instead being targeted for degradation.

In conclusion, we discovered a unique endorepellin-dependent transcriptomic signature revealing a broad remodeling of genes to favor the autophagic response. Furthermore, for the first time, we found evidence of endorepellin regulating mitochondrial dynamics. These findings have widened our understanding of matrix-driven autophagy and provide a framework

conducive for a deeper understanding of this conserved process.

### Experimental procedures

#### Cells, chemicals, and reagents

HUVEC were obtained from Lifeline Cell Technology (Frederick, MD), grown in basal medium and supplemented with the Vasculife EnGS LifeFactors Kit (Lifeline Cell Technology). HUVEC were used within the first five passages. Telo-HAEC were obtained from American Type Cell Cultures (Manassas, VA) and cultured in EGM-2 SingleQuot Kit Supplements and Growth Factors (Lonza). Rabbit polyclonal antibodies against GAPDH, PINK1, VEGFR2, and p62/SQSTM1 were obtained from Cell Signaling Technology. Rabbit polyclonal anti-LC3B, SU5416, CCCP, FCCP, and JC-1 were purchased from Sigma. The horseradish peroxidase-conjugated goat anti-rabbit, donkey anti-mouse secondary antibodies, and negative rabbit and mouse IgG-G2 immunoprecipitation antibodies were obtained from EMD Millipore (Billerica, MA). Mouse monoclonal antibodies against Parkin and mitofusin 2 were obtained from Cell Signaling Technology. Mouse mAb against  $\alpha$ -tubulin was purchased from Santa Cruz Biotechnology. A custom rabbit polyclonal antibody against mitostatin was generated as described elsewhere (73). All primary antibodies were used at 1:1000 dilution in 1% BSA/TBST, except for GAPDH, which was used at 1:10,000 and  $\alpha$ -tubulin, which was used at 1:400. For immunofluorescence, primary antibodies were used at 1:200 in 1% BSA in PBS. Secondary antibodies for chemiluminescence were used at 1:5,000 in the same buffer as above. SuperSignal West Pico enhanced chemiluminescence substrate was purchased from Thermo Fisher Scientific. The purification and validation of human recombinant endorepellin have been described and demonstrated above. Purification and validation of human recombinant LG1/2 and LG3 are described elsewhere (51). Highly purified endorepellin was used at 200 nM, whereas LG1/2 and LG3 was used at 150 nM throughout the study. Original, whole blots can be found in Fig. S3.

#### NanoString transcriptomic analysis

NanoString nCounter reporter probe-sets were designed to detect expression changes in a manually curated set ( $n = 95$ ) of established autophagy genes available in the literature at the time of probe-set synthesis.

Early passage HUVEC (P3) were treated ( $n = 6$ ) with vehicle (PBS) or endorepellin (6 h, 200 nM). RNA was extracted and validated by an Agilent 2200 TapeStation before entering the workflow for NanoString analyses. Samples were processed (including RNA validation) at the Genomic Pathology Laboratory (Thomas Jefferson University), following the nCounter Gene Expression protocol. Briefly, total RNA was incubated at 65 °C with reporter and capture probes in hybridization buffer. Capture probes were purified and analyzed on the nCounter Digital Analyzer. The number of molecules of a given transcript in the endorepellin-treated samples was determined by normalizing detected transcript counts to the geometric mean of control RNA sequences and a set of control genes ( $n = 5$ ) that did not show evidence of altered expression by endorepellin. Significant differences between vehicle and endorepellin ( $p <$



0.05) were detected by paired two-tailed *t* tests comparing the paired mean values for each gene (averaged across samples within each condition) between each condition.

### Transient RNAi-mediated silencing

HUVEC were transiently transfected using Lipofectamine RNAiMAX (Life Technologies) mixed with siRNA against *Homo sapiens VEGFR2* (Santa Cruz Biotechnology). Scrambled siRNA (Santa Cruz Biotechnology) served as a control for all siRNA experiments presented herein. The protocol for siRNA-mediated silencing is described elsewhere (99).

### Mitochondrial membrane potential

At least three individual assays were performed in HUVEC using the mitochondrial dye JC-1. HUVEC were grown in four chambered glass slides coated with 0.1% gelatin for 24 h at 37 °C. Cells were treated as per the experimental conditions described herein. CCCP was used at 30 μM and FCCP used at 500 nM for the last hour or 10 min before staining with JC-1, respectively. Each chamber was incubated with JC-1 (7.5 μM) for 20 min. Cells were washed three times with PBS and imaged live using a Leica DM5500B microscope. All the images were procured using the same exposure, gain, and intensity.

### Immunofluorescence and confocal laser microscopy

Typically,  $\sim 5 \times 10^4$  HUVEC were plated on 0.2% gelatin-coated 4-well chamber slides (Nunc, Thermo Scientific) and grown to full confluence in their growth media at 37 °C. Cells were treated as per the experimental conditions contained herein, and immunofluorescence was performed as previously done (100, 101). Slides were incubated with conjugated secondary antibodies such as: goat anti-rabbit IgG Alexa Fluor® 488 and goat anti-mouse IgG Alexa Fluor® 564 (Invitrogen). Nuclei were visualized with 4',6-diamidino-2-phenylindole (Vector Laboratories). JC-1 live cell immunofluorescence images were acquired with a  $\times 10$  objective on a LEICA DM5500B microscope installed with the Leica Application suite, using advanced fluorescence version 1.8 software (Leica Microsystems, Frankfurt, Germany). Confocal analyses were carried out utilizing a  $\times 63$ , 1.3 oil-immersion objective of a Zeiss LSM-780 confocal laser-scanning microscope with Zen Imaging Software. A full description of the immunofluorescence and confocal laser microscopy protocol can be found elsewhere (78).

### Quantitative real-time PCR

Expression analysis by quantitative real-time PCR was carried out on subconfluent six-well plates seeded with  $\sim 2 \times 10^5$  of HUVEC and harvested in TRIzol reagent (Invitrogen) following the appropriate experimental conditions. Gene expression analysis was performed on a Roche LightCycler 480-II and calculated with the comparative  $C_t$  method. A full description can be found in Ref. 26.

### Quantification and statistical analysis

Immunoblots were quantified by scanning densitometry using Scion ImageJ software (NIH). Graphs were generated using Sigma Stat 3.10. Experiments with three or more comparison groups were subjected to one-way ANOVA followed by a

Bonferroni post hoc test. Differences among the conditions were considered significant at  $p < 0.05$ .

*Author contributions*—T. N. and R. V. I. conceptualization; T. N. and R. V. I. data curation; T. N. and R. V. I. formal analysis; T. N. and R. V. I. writing-original draft; T. N. and R. V. I. writing-review and editing; E. A., Z.-X. W., S. C. P., and M. M. resources; Z.-X. W. and S. C. P. methodology; S. C. P. and R. V. I. funding acquisition.

*Acknowledgments*—We thank Carolyn Chen and Aastha Kapoor for providing the purified human recombinant endorepellin. We thank all members of the Iozzo laboratory for valuable discussions and suggestions.

### References

- Cohen, I. R., Murdoch, A. D., Naso, M. F., Marchetti, D., Berd, D., and Iozzo, R. V. (1994) Abnormal expression of perlecan proteoglycan in metastatic melanomas. *Cancer Res.* **54**, 5771–5774 [Medline](#)
- Iozzo, R. V., and Schaefer, L. (2015) Proteoglycan form and function: a comprehensive nomenclature of proteoglycans. *Matrix Biol.* **42**, 11–55 [CrossRef Medline](#)
- Neill, T., Schaefer, L., and Iozzo, R. V. (2014) Instructive roles of extracellular matrix on autophagy. *Am. J. Pathol.* **184**, 2146–2153 [CrossRef Medline](#)
- Poluzzi, C., Iozzo, R. V., and Schaefer, L. (2016) Endostatin and endorepellin: a common route of action for similar angiostatic cancer avengers. *Adv. Drug Deliv. Rev.* **97**, 156–173 [CrossRef Medline](#)
- Schaefer, L., Tredup, C., Gubbiotti, M. A., and Iozzo, R. V. (2017) Proteoglycan neofunctions: regulation of inflammation and autophagy in cancer biology. *FEBS J.* **284**, 10–26 [CrossRef Medline](#)
- Nguyen, T. M., Subramanian, I. V., Xiao, X., Ghosh, G., Nguyen, P., Kelekar, A., and Ramakrishnan, S. (2009) Endostatin induces autophagy in endothelial cells by modulating Beclin 1 and  $\beta$ -catenin levels. *J. Cell. Mol. Med.* **13**, 3687–3698 [CrossRef Medline](#)
- Nyström, A., Bornert, O., and Köhl, T. (2017) Cell therapy for basement membrane-linked diseases. *Matrix Biol.* **57**, 124–139 [Medline](#)
- Aviezer, D., Hecht, D., Safran, M., Eisinger, M., David, G., and Yayon, A. (1994) Perlecan, basal lamina proteoglycan, promotes basic fibroblast growth factor-receptor binding, mitogenesis, and angiogenesis. *Cell* **79**, 1005–1013 [CrossRef Medline](#)
- Iozzo, R. V., and Cohen, I. (1993) Altered proteoglycan gene expression and the tumor stroma. *Experientia* **49**, 447–455 [CrossRef Medline](#)
- Fuki, I. V., Iozzo, R. V., and Williams, K. J. (2000) Perlecan heparan sulfate proteoglycan: a novel receptor that mediates a distinct pathway for ligand catabolism. *J. Biol. Chem.* **275**, 25742–25750 [CrossRef Medline](#)
- Ghadiali, R. S., Guimond, S. E., Turnbull, J. E., and Piscitoni, A. (2017) Dynamic changes in heparan sulfate during muscle differentiation and ageing regulate myoblast cell fate and FGF2 signalling. *Matrix Biol.* **59**, 54–68 [CrossRef Medline](#)
- Iozzo, R. V. (2005) Basement membrane proteoglycans: from cellar to ceiling. *Nat. Rev. Mol. Cell Biol.* **6**, 646–656 [CrossRef Medline](#)
- Farach-Carson, M. C., Warren, C. R., Harrington, D. A., and Carson, D. D. (2014) Border patrol: insights into the unique role of perlecan/heparan sulfate proteoglycan 2 at cell and tissue borders. *Matrix Biol.* **34**, 64–79 [CrossRef Medline](#)
- Naba, A., Clauser, K. R., Ding, H., Whittaker, C. A., Carr, S. A., and Hynes, R. O. (2016) The extracellular matrix: Tools and insights for the “omics” era. *Matrix Biol.* **49**, 10–24 [CrossRef Medline](#)
- Randles, M. J., Humphries, M. J., and Lennon, R. (2017) Proteomic definitions of basement membrane composition in health and disease. *Matrix Biol.* **57**, 12–28 [Medline](#)
- Pozzi, A., Yurchenco, P. D., and Iozzo, R. V. (2017) The nature and biology of basement membranes. *Matrix Biol.* **57**, 1–11 [Medline](#)
- Foster, M. H. (2017) Basement membranes and autoimmune diseases. *Matrix Biol.* **57**, 149–168 [Medline](#)

## Endorepellin evokes a pro-autophagic gene signature

18. Wilson, S. E., Marino, G. K., Torricelli, A. A. M., and Medeiros, C. S. (2017) Injury and defective regeneration of the epithelial basement membrane in corneal fibrosis: a paradigm for fibrosis in other organs? *Matrix Biol.* **64**, 17–26 [CrossRef Medline](#)
19. Wijeratne, S. S., Martinez, J. R., Grindel, B. J., Frey, E. W., Li, J., Wang, K., Farach-Carson, M. C., and Kiang, C. H. (2016) Single molecule force measurements of perlecan/HSPG2: a key component of the osteocyte pericellular matrix. *Matrix Biol.* **50**, 27–38 [CrossRef Medline](#)
20. Peysseon, F., and Ricard-Blum, S. (2014) Heparin-protein interactions: from affinity and kinetics to biological roles: application to an interaction network regulating angiogenesis. *Matrix Biol.* **35**, 73–81 [CrossRef Medline](#)
21. Gubbiotti, M. A., Neill, T., and Iozzo, R. V. (2017) A current view of perlecan in physiology and pathology: a mosaic of functions. *Matrix Biol.* **57**, 285–298 [Medline](#)
22. Tanimoto, R., Palladino, C., Xu, S. Q., Buraschi, S., Neill, T., Gomella, L. G., Peiper, S. C., Belfiore, A., Iozzo, R. V., and Morrione, A. (2017) The perlecan-interacting growth factor progranulin regulates ubiquitination, sorting, and lysosomal degradation of sortilin. *Matrix Biol.* **64**, 27–39 [CrossRef Medline](#)
23. Mongiat, M., Sweeney, S. M., San Antonio, J. D., Fu, J., and Iozzo, R. V. (2003) Endorepellin, a novel inhibitor of angiogenesis derived from the C terminus of perlecan. *J. Biol. Chem.* **278**, 4238–4249 [CrossRef Medline](#)
24. Iozzo, R. V., and San Antonio, J. D. (2001) Heparan sulfate proteoglycans: heavy hitters in the angiogenesis arena. *J. Clin. Invest.* **108**, 349–355 [CrossRef Medline](#)
25. Lord, M. S., Chuang, C. Y., Melrose, J., Davies, M. J., Iozzo, R. V., and Whitelock, J. M. (2014) The role of vascular-derived perlecan in modulating cell adhesion, proliferation and growth factor signaling. *Matrix Biol.* **35**, 112–122 [CrossRef Medline](#)
26. Yang, Y., Xu, W., Neill, T., Hu, Z., Wang, C. H., Xiao, X., Stock, S., Guise, T., Yun, C. O., Brendler, C. B., Iozzo, R. V., and Seth, P. (2015) Systemic delivery of an oncolytic adenovirus expressing decorin for the treatment of breast cancer bone metastases. *Hum. Gene Ther.* **26**, 813–825 [CrossRef Medline](#)
27. Jung, M., Lord, M. S., Cheng, B., Lyons, J. G., Alkhoury, H., Hughes, J. M., McCarthy, S. J., Iozzo, R. V., and Whitelock, J. M. (2013) Mast cells produce novel shorter forms of perlecan that contain functional endorepellin: a role in angiogenesis and wound healing. *J. Biol. Chem.* **288**, 3289–3304 [CrossRef Medline](#)
28. Arpino, V., Brock, M., and Gill, S. E. (2015) The role of TIMPs in regulation of extracellular matrix proteolysis. *Matrix Biol.* **44**, 247–254 [Medline](#)
29. Wells, J. M., Gaggari, A., and Blalock, J. E. (2015) MMP generated matrikines. *Matrix Biol.* **44**, 122–129 [Medline](#)
30. Deryugina, E. I., and Quigley, J. P. (2015) Tumor angiogenesis: MMP-mediated induction of intravasation- and metastasis-sustaining neovasculation. *Matrix Biol.* **44**, 94–112 [Medline](#)
31. Vadon-Le Goff, S., Hulmes, D. J., and Moali, C. (2015) BMP-1/tolloid-like proteinases synchronize matrix assembly with growth factor activation to promote morphogenesis and tissue remodeling. *Matrix Biol.* **44**, 14–23 [Medline](#)
32. Apte, S. S., and Parks, W. C. (2015) Metalloproteinases: A parade of functions in matrix biology and an outlook for the future. *Matrix Biol.* **44**, 1–6 [Medline](#)
33. Rohani, M. G., and Parks, W. C. (2015) Matrix remodelling by MMPs during wound repair. *Matrix Biol.* **44**, 113–121 [Medline](#)
34. Duarte, S., Baber, J., Fujii, T., and Coito, A. J. (2015) Matrix metalloproteinases in liver injury, repair and fibrosis. *Matrix Biol.* **44**, 147–156 [Medline](#)
35. Andreuzzi, E., Colladel, R., Pellicani, R., Tarticchio, G., Cannizzaro, R., Spessotto, P., Bussolati, B., Brossa, A., De Paoli, P., Canzonieri, V., Iozzo, R. V., Colombatti, A., and Mongiat, M. (2017) The angiostatic molecule Multimerin 2 is processed by MMP-9 to allow sprouting angiogenesis. *Matrix Biol.* **64**, 40–53 [CrossRef Medline](#)
36. Gonzalez, E. M., Reed, C. C., Bix, G., Fu, J., Zhang, Y., Gopalakrishnan, B., Greenspan, D. S., and Iozzo, R. V. (2005) BMP-1/Tolloid-like metalloproteases process endorepellin, the angiostatic C-terminal fragment of perlecan. *J. Biol. Chem.* **280**, 7080–7087 [CrossRef Medline](#)
37. Le, B. V., Kim, H., Choi, J., Kim, J.-H., Hahn, M.-J., Lee, C., Kim, K. K., and Hwang, H.-Y. (2011) Crystal structure of the LG3 domain of endorepellin, an angiogenesis inhibitor. *J. Mol. Biol.* **414**, 231–242 [CrossRef Medline](#)
38. Parker, T. J., Sampson, D. L., Broszczak, D., Chng, Y. L., Carter, S. L., Leavesley, D. I., Parker, A. W., and Upton, Z. (2012) A fragment of the LG3 peptide of endorepellin is present in the urine of physically active mining workers: a potential marker of physical activity. *PLoS ONE* **7**, e33714 [CrossRef Medline](#)
39. Oda, O., Shinzato, T., Ohbayashi, K., Takai, I., Kunimatsu, M., Maeda, K., and Yamanaka, N. (1996) Purification and characterization of perlecan fragment in urine of end-stage renal failure patients. *Clin. Chim. Acta* **255**, 119–132 [CrossRef Medline](#)
40. Vuadens, F., Benay, C., Crettaz, D., Gallot, D., Sapin, V., Schneider, P., Binevenut, W.-V., Lémy, D., Quadroni, M., Dastugue, B., and Tissot, J.-D. (2003) Identification of biologic markers of the premature rupture of fetal membranes: proteomic approach. *Proteomics* **3**, 1521–1525 [CrossRef Medline](#)
41. O’Riordan, E., Orlova, T. N., Mendelev, N., Patschan, D., Kemp, R., Chander, P. N., Hu, R., Hao, G., Gross, S. S., Iozzo, R. V., Delaney, V., and Goligorsky, M. S. (2008) Urinary proteomic analysis of chronic renal allograft nephropathy. *Proteomics Clin. Appl.* **2**, 1025–1035 [CrossRef Medline](#)
42. Thadikkaran, L., Crettaz, D., Siegenthaler, M. A., Gallot, D., Sapin, V., Iozzo, R. V., Queloz, P. A., Schneider, P., and Tissot, J. D. (2005) The role of proteomics in the assessment of premature rupture of fetal membranes. *Clin. Chim. Acta* **360**, 27–36 [CrossRef Medline](#)
43. Mauri, P., Scarpa, A., Nascimbeni, A. C., Benazzi, L., Parmagnani, E., Mafficini, A., Della Peruta, M., Bassi, C., Miyazaki, K., and Sorio, C. (2005) Identification of proteins released by pancreatic cancer cells by multidimensional protein identification technology: a strategy for identification of novel cancer markers. *FASEB J.* **19**, 1125–1127 [CrossRef Medline](#)
44. Gronborg, M., Kristiansen, T. Z., Iwahori, A., Chang, R., Reddy, R., Sato, N., Molina, H., Jensen, O. N., Hruban, R. H., Goggins, M. G., Maitra, A., and Pandey, A. (2006) Biomarker discovery from pancreatic cancer secretome using a differential proteomic approach. *Mol. Cell. Proteomics* **5**, 157–171 [CrossRef](#)
45. Tsangaris, G. T., Karamessinis, P., Kolialexi, A., Garbis, S. D., Antsaklis, A., Mavrou, A., and Fountoulakis, M. (2006) Proteomic analysis of amniotic fluid in pregnancies with Down syndrome. *Proteomics* **6**, 4410–4419 [CrossRef Medline](#)
46. Aspinall-O’Dea, M., and Costello, E. (2007) The pancreatic cancer proteome—recent advances and future promise. *Proteomics Clin. Appl.* **1**, 1066–1079 [CrossRef Medline](#)
47. Májek, P., Reichelová, Z., Suttner, J., Cermák, J., and Dyr, J. E. (2011) Plasma proteome changes associated with refractory cytopenia with multilineage dysplasia. *Proteome Sci.* **9**, 64 [CrossRef Medline](#)
48. Surin, B., Sachon, E., Rougier, J.-P., Steverlyncq, C., Garreau, C., Lelongt, B., Ronco, P., and Piedagnel, R. (2013) LG3 fragment of endorepellin is a possible biomarker of severity in IgA nephropathy. *Proteomics* **13**, 142–152 [CrossRef Medline](#)
49. Chang, J. W., Kang, U.-B., Kim, D. H., Yi, J. K., Lee, J. W., Noh, D.-Y., Lee, C., and Yu, M.-H. (2008) Identification of circulating endorepellin LG3 fragment: potential use as a serological biomarker for breast cancer. *Proteomics Clin. Appl.* **2**, 23–32 [CrossRef Medline](#)
50. Goyal, A., Pal, N., Concannon, M., Paul, M., Doran, M., Poluzzi, C., Sekiguchi, K., Whitelock, J. M., Neill, T., and Iozzo, R. V. (2011) Endorepellin, the angiostatic module of perlecan, interacts with both the  $\alpha 2\beta 1$  integrin and vascular endothelial growth factor receptor 2 (VEGFR2). *J. Biol. Chem.* **286**, 25947–25962 [CrossRef Medline](#)
51. Willis, C. D., Poluzzi, C., Mongiat, M., and Iozzo, R. V. (2013) Endorepellin laminin-like globular repeat 1/2 domains bind Ig3–5 of vascular endothelial growth factor (VEGF) receptor 2 and block pro-angiogenic signaling by VEGFA in endothelial cells. *FEBS J.* **280**, 2271–2284 [CrossRef Medline](#)

52. Douglass, S., Goyal, A., and Iozzo, R. V. (2015) The role of perlecan and endorepellin in the control of tumor angiogenesis and endothelial cell autophagy. *Connect. Tissue Res.* **56**, 381–391 [CrossRef Medline](#)
53. Poluzzi, C., Casulli, J., Goyal, A., Mercer, T. J., Neill, T., and Iozzo, R. V. (2014) Endorepellin evokes autophagy in endothelial cells. *J. Biol. Chem.* **289**, 16114–16128 [CrossRef Medline](#)
54. Goyal, A., Poluzzi, C., Willis, C. D., Smythies, J., Shellard, A., Neill, T., and Iozzo, R. V. (2012) Endorepellin affects angiogenesis by antagonizing diverse VEGFR2-evoked signaling pathways: transcriptional repression of HIF-1 $\alpha$  and VEGFA and concurrent inhibition of NFAT1 activation. *J. Biol. Chem.* **287**, 43543–43556 [CrossRef Medline](#)
55. Goyal, A., Gubbiotti, M. A., Chery, D. R., Han, L., and Iozzo, R. V. (2016) Endorepellin-evoked autophagy contributes to angiostasis. *J. Biol. Chem.* **291**, 19245–19256 [CrossRef Medline](#)
56. Füllgrabe, J., Klionsky, D. J., and Joseph, B. (2014) The return of the nucleus: transcriptional and epigenetic control of autophagy. *Nat. Rev. Mol. Cell Biol.* **15**, 65–74 [CrossRef Medline](#)
57. Füllgrabe, J., Lynch-Day, M. A., Heldring, N., Li, W., Struijk, R. B., Ma, Q., Hermanson, O., Rosenfeld, M. G., Klionsky, D. J., and Joseph, B. (2013) The histone H4 lysine acetyltransferase hMOF regulates the outcome of autophagy. *Nature* **500**, 468–471 [CrossRef Medline](#)
58. Seok, S., Fu, T., Choi, S. E., Li, Y., Zhu, R., Kumar, S., Sun, X., Yoon, G., Kang, Y., Zhong, W., Ma, J., Kemper, B., and Kemper, J. K. (2014) Transcriptional regulation of autophagy by an FXR-CREB axis. *Nature* **516**, 108–111 [Medline](#)
59. Nussenzweig, S. C., Verma, S., and Finkel, T. (2015) The role of autophagy in vascular biology. *Circ. Res.* **116**, 480–488 [CrossRef Medline](#)
60. Gabel, H. W., Kinde, B., Stroud, H., Gilbert, C. S., Harmin, D. A., Kastan, N. R., Hemberg, M., Ebert, D. H., and Greenberg, M. E. (2015) Disruption of DNA-methylation-dependent long gene repression in Rett syndrome. *Nature* **522**, 89–93 [CrossRef Medline](#)
61. Naik, S., Bouladoux, N., Linehan, J. L., Han, S. J., Harrison, O. J., Wilhelm, C., Conlan, S., Himmelfarb, S., Byrd, A. L., Deming, C., Quinones, M., Brenchley, J. M., Kong, H. H., Tussiwand, R., Murphy, K. M., Merad, M., Segre, J. A., and Belkaid, Y. (2015) Commensal-dendritic-cell interaction specifies a unique protective skin immune signature. *Nature* **520**, 104–108 [CrossRef Medline](#)
62. Hong, M., Sandalova, E., Low, D., Gehring, A. J., Fieni, S., Amadei, B., Urbani, S., Chong, Y. S., Guccione, E., and Bertoletti, A. (2015) Trained immunity in newborn infants of HBV-infected mothers. *Nat. Commun.* **6**, 6588 [CrossRef Medline](#)
63. Wang, H., Yu, C., Gao, X., Welte, T., Muscarella, A. M., Tian, L., Zhao, H., Zhao, Z., Du, S., Tao, J., Lee, B., Westbrook, T. F., Wong, S. T., Jin, X., Rosen, J. M., Osborne, C. K., and Zhang, X. H. (2015) The osteogenic niche promotes early-stage bone colonization of disseminated breast cancer cells. *Cancer Cell* **27**, 193–210 [CrossRef Medline](#)
64. Pattingre, S., Tassa, A., Qu, X., Garuti, R., Liang, X. H., Mizushima, N., Packer, M., Schneider, M. D., and Levine, B. (2005) Bcl-2 antiapoptotic proteins inhibit Beclin 1-dependent autophagy. *Cell* **122**, 927–939 [CrossRef Medline](#)
65. Pattingre, S., and Levine, B. (2006) Bcl-2 inhibition of autophagy: a new route to cancer? *Cancer Res.* **66**, 2885–2888 [CrossRef Medline](#)
66. Narendra, D., Walker, J. E., and Youle, R. (2012) Mitochondrial quality control mediated by PINK1 and Parkin: links to parkinsonism. *Cold Spring Harb. Perspect. Biol.* **4**, a011338 [Medline](#)
67. Vecchione, A., Fassan, M., Anesti, V., Morrione, A., Goldoni, S., Baldassarre, G., Byrne, D., D'Arca, D., Palazzo, J. P., Lloyd, J., Scorrano, L., Gomella, L. G., Iozzo, R. V., and Baffa, R. (2009) MITOSTATIN, a putative tumor suppressor on chromosome 12q24.1, is downregulated in human bladder and breast cancer. *Oncogene* **28**, 257–269 [CrossRef Medline](#)
68. Fassan, M., D'Arca, D., Letko, J., Vecchione, A., Gardiman, M. P., McCue, P., Wildemore, B., Ruge, M., Shupp-Byrne, D., Gomella, L. G., Morrione, A., Iozzo, R. V., and Baffa, R. (2011) Mitostatin is down-regulated in human prostate cancer and suppresses the invasive phenotype of prostate cancer cells. *PLoS ONE* **6**, e19771 [CrossRef Medline](#)
69. Vincow, E. S., Merrihew, G., Thomas, R. E., Shulman, N. J., Beyer, R. P., MacCoss, M. J., and Pallanck, L. J. (2013) The PINK1-Parkin pathway promotes both mitophagy and selective respiratory chain turnover *in vivo*. *Proc. Natl. Acad. Sci. U.S.A.* **110**, 6400–6405 [CrossRef Medline](#)
70. Chan, N. C., Salazar, A. M., Pham, A. H., Sweredoski, M. J., Kolawa, N. J., Graham, R. L., Hess, S., and Chan, D. C. (2011) Broad activation of the ubiquitin-proteasome system by Parkin is critical for mitophagy. *Hum. Mol. Genet.* **20**, 1726–1737 [CrossRef Medline](#)
71. Geisler, S., Holmström, K. M., Skujat, D., Fiesel, F. C., Rothfuss, O. C., Kahle, P. J., and Springer, W. (2010) PINK1/Parkin-mediated mitophagy is dependent on VDAC1 and p62/SQSTM1. *Nat. Cell Biol.* **12**, 119–131 [CrossRef Medline](#)
72. Sun, Y., Vashisht, A. A., Tchiew, J., Wohlschlegel, J. A., and Dreier, L. (2012) Voltage-dependent anion channels (VDACs) recruit Parkin to defective mitochondria to promote mitochondrial autophagy. *J. Biol. Chem.* **287**, 40652–40660 [CrossRef Medline](#)
73. Neill, T., Torres, A., Buraschi, S., Owens, R. T., Hoek, J. B., Baffa, R., and Iozzo, R. V. (2014) Decorin induces mitophagy in breast carcinoma cells via peroxisome proliferator-activated receptor  $\gamma$  coactivator-1 $\alpha$  (PGC-1 $\alpha$ ) and mitostatin. *J. Biol. Chem.* **289**, 4952–4968 [CrossRef Medline](#)
74. Nyström, A., Shaik, Z. P., Gullberg, D., Krieg, T., Eckes, B., Zent, R., Pozzi, A., and Iozzo, R. V. (2009) Role of tyrosine phosphatase SHP-1 in the mechanism of endorepellin angiostatic activity. *Blood* **114**, 4897–4906 [CrossRef Medline](#)
75. Neill, T., Schaefer, L., and Iozzo, R. V. (2015) Decoding the matrix: instructive roles of proteoglycan receptors. *Biochemistry* **54**, 4583–4598 [CrossRef Medline](#)
76. Mendel, D. B., Schreck, R. E., West D. C., Li, G., Strawn, L. M., Tanciongco, S. S., Vasile, S., Shawver, L. K., and Cherrington, J. M. (2000) The angiogenesis inhibitor SU5416 has long-lasting effects on vascular endothelial growth factor receptor phosphorylation and function. *Clin. Cancer Res.* **6**, 4848–4858 [Medline](#)
77. Fong, T. A., Shawver, L. K., Sun, L., Tang, C., App, H., Powell, T. J., Kim, Y. H., Schreck, R., Wang, X., Risau, W., Ullrich, A., Hirth, K. P., and McMahon, G. (1999) SU5416 is a potent and selective inhibitor of the vascular endothelial growth factor receptor (Flk-1/KDR) that inhibits tyrosine kinase catalysis, tumor vascularization, and growth of multiple tumor types. *Cancer Res.* **59**, 99–106 [Medline](#)
78. Neill, T., Buraschi, S., Goyal, A., Sharpe, C., Natkanski, E., Schaefer, L., Morrione, A., and Iozzo, R. V. (2016) EphA2 is a functional receptor for the growth factor progranulin. *J. Cell Biol.* **215**, 687–703 [CrossRef Medline](#)
79. Narendra, D. P., Jin, S. M., Tanaka, A., Suen, D. F., Gautier, C. A., Shen, J., Cookson, M. R., and Youle, R. J. (2010) PINK1 is selectively stabilized on impaired mitochondria to activate Parkin. *PLoS Biol.* **8**, e1000298 [CrossRef Medline](#)
80. Narendra, D., Tanaka, A., Suen, D. F., and Youle, R. J. (2008) Parkin is recruited selectively to impaired mitochondria and promotes their autophagy. *J. Cell Biol.* **183**, 795–803 [CrossRef Medline](#)
81. Cossarizza, A., Baccarani-Contri, M., Kalashnikova, G., and Franceschi, C. (1993) A new method for the cytofluorimetric analysis of mitochondrial membrane potential using the J-aggregate forming lipophilic cation 5,5',6,6'-tetrachloro-1,1',3,3'-tetraethylbenzimidazolcarbocyanine iodide (JC-1). *Biochem. Biophys. Res. Commun.* **197**, 40–45 [CrossRef Medline](#)
82. Willis, C. D., Schaefer, L., and Iozzo, R. V. (2012) The biology of perlecan and its bioactive modules (Karamanos, N. K., ed) in *Extracellular Matrix: Pathobiology and Signaling*, Walter de Gruyter GmbH & Co. KG, Berlin
83. Bix, G., Fu, J., Gonzalez, E. M., Macro, L., Barker, A., Campbell, S., Zutter, M. M., Santoro, S. A., Kim, J. K., Höök, M., Reed, C. C., and Iozzo, R. V. (2004) Endorepellin causes endothelial cell disassembly of actin cytoskeleton and focal adhesions through the  $\alpha 2\beta 1$  integrin. *J. Cell Biol.* **166**, 97–109 [CrossRef Medline](#)
84. Yamano, K., and Youle, R. J. (2013) PINK1 is degraded through the N-end rule pathway. *Autophagy* **9**, 1758–1769 [CrossRef Medline](#)
85. Chen, Y., and Dorn, G. W., 2nd (2013) PINK1-phosphorylated mitofusin 2 is a Parkin receptor for culling damaged mitochondria. *Science* **340**, 471–475 [CrossRef Medline](#)
86. Cerqua, C., Anesti, V., Pyakurel, A., Liu, D., Naon, D., Wiche, G., Baffa, R., Dimmer, K. S., and Scorrano, L. (2010) Trichoplein/mitostatin regulates



## Endorepellin evokes a pro-autophagic gene signature

- endoplasmic reticulum-mitochondria juxtaposition. *EMBO Rep.* **11**, 854–860 [CrossRef Medline](#)
87. Mizushima, N., Yoshimori, T., and Levine, B. (2010) Methods in mammalian autophagy research. *Cell* **140**, 313–326 [CrossRef Medline](#)
88. Liang, X. H., Jackson, S., Seaman, M., Brown, K., Kempkes, B., Hibshoosh, H., and Levine, B. (1999) Induction of autophagy and inhibition of tumorigenesis by *beclin 1*. *Nature* **402**, 672–676 [CrossRef Medline](#)
89. Yue, Z., Jin, S., Yang, C., Levine, A. J., and Heintz, N. (2003) Beclin 1, an autophagy gene essential for early embryonic development, is a haploinsufficient tumor suppressor. *Proc. Natl. Acad. Sci. U.S.A.* **100**, 15077–15082 [CrossRef Medline](#)
90. Wang, R. C., Wei, Y., An, Z., Zou, Z., Xiao, G., Bhagat, G., White, M., Reichelt, J., and Levine, B. (2012) Akt-mediated regulation of autophagy and tumorigenesis through Beclin 1 phosphorylation. *Science* **338**, 956–959 [CrossRef Medline](#)
91. Wei, Y., Zou, Z., Becker, N., Anderson, M., Sumpter, R., Xiao, G., Kinch, L., Koduru, P., Christudass, C. S., Veltri, R. W., Grishin, N. V., Peyton, M., Minna, J., Bhagat, G., and Levine, B. (2013) EGFR-mediated beclin 1 phosphorylation in autophagy suppression, tumor progression, and tumor chemoresistance. *Cell* **154**, 1269–1284 [CrossRef Medline](#)
92. Gubbiotti, M. A., and Iozzo, R. V. (2015) Proteoglycans regulate autophagy via outside-in signaling: an emerging new concept. *Matrix Biol.* **48**, 6–13 [CrossRef Medline](#)
93. He, C., Wei, Y., Sun, K., Li, B., Dong, X., Zou, Z., Liu, Y., Kinch, L. N., Khan, S., Sinha, S., Xavier, R. J., Grishin, N. V., Xiao, G., Eskelinen, E. L., Scherer, P. E., Whistler, J. L., and Levine, B. (2013) Beclin 2 functions in autophagy, degradation of G protein-coupled receptors, and metabolism. *Cell* **154**, 1085–1099 [CrossRef Medline](#)
94. Matsuda, N., Sato, S., Shiba, K., Okatsu, K., Saisho, K., Gautier, C. A., Sou, Y. S., Saiki, S., Kawajiri, S., Sato, F., Kimura, M., Komatsu, M., Hattori, N., and Tanaka, K. (2010) PINK1 stabilized by mitochondrial depolarization recruits Parkin to damaged mitochondria and activates latent Parkin for mitophagy. *J. Cell Biol.* **189**, 211–221 [CrossRef Medline](#)
95. Simons, M., Gordon, E., and Claesson-Welsh, L. (2016) Mechanisms and regulation of endothelial VEGF receptor signalling. *Nat. Rev. Mol. Cell Biol.* **17**, 611–625 [CrossRef Medline](#)
96. Wolf, S. G., Mutsafi, Y., Dadosh, T., Ilani, T., Lansky, Z., Horowitz, B., Rubin, S., Elbaum, M., and Fass, D. (2017) 3D visualization of mitochondrial solid-phase calcium stores in whole cells. *Elife* **6**, e29929 [CrossRef Medline](#)
97. Pallanck, L. (2013) Mitophagy: mitofusins recruits a mitochondrial killer. *Curr. Biol.* **23**, R570–R572 [CrossRef Medline](#)
98. Song, W. H., Yi, Y. J., Sutovsky, M., Meyers, S., and Sutovsky, P. (2016) Autophagy and ubiquitin-proteasome system contribute to sperm mitophagy after mammalian fertilization. *Proc. Natl. Acad. Sci. U.S.A.* **113**, E5261–E5270 [CrossRef Medline](#)
99. Neill, T., Painter, H., Buraschi, S., Owens, R. T., Lisanti, M. P., Schaefer, L., and Iozzo, R. V. (2012) Decorin antagonizes the angiogenic network: concurrent inhibition of Met, hypoxia inducible factor-1 $\alpha$  and vascular endothelial growth factor A and induction of thrombospondin-1 and TIMP3. *J. Biol. Chem.* **287**, 5492–5506 [CrossRef Medline](#)
100. Rudnicka, L., Varga, J., Christiano, A. M., Iozzo, R. V., Jimenez, S. A., and Uitto, J. (1994) Elevated expression of type VII collagen in the skin of patients with systemic sclerosis. *J. Clin. Invest.* **93**, 1709–1715 [CrossRef Medline](#)
101. Ryyänen, M., Ryyänen, J., Sollberg, S., Iozzo, R. V., Knowlton, R. G., and Uitto, J. (1992) Genetic linkage of Type VII collagen (COL7A1) to dominant dystrophic epidermolysis bullosa in families with abnormal anchoring fibrils. *J. Clin. Invest.* **89**, 974–980 [CrossRef Medline](#)